Phys Chem Minerals (1999) 26: 633–643

ORIGINAL PAPER

H. Xu · P.J. Heaney · H. Böhm

Structural modulations and phase transitions in β-eucryptite: an in-situ TEM study

Received: 12 November 1998 / Revised and accepted: 31 December 1998

Abstract Beta-eucryptite as grown by the flux method has been investigated by in-situ cold- and hot-stage transmission electron microscopy (TEM). Using electron diffraction and dark-field TEM imaging, we found no evidence for the merohedral twinning that accompanies structural collapse at the β-to-α-quartz transition, suggesting a true hexagonal symmetry for the aluminosilicate framework of β-eucryptite. Selected-area electron diffraction (SAED) patterns exhibited a variety of incommensurate structures along the three **a** axes with an average modulation period of about 6.5 **a**. These modulated structures arise from superperiodic stacking parallel to (100) of two structural units with different Li configurations. In-situ heating experiments show that the modulated structures undergo a reversible transition to the disordered modification at elevated temperatures. This transition arises from positional order-disorder of Li ions along the main structural channels. In addition, it appears that at constant low temperature, electron beam irradiation alone can induce a sequence of transitions similar to those that are thermally induced from the ordered modification to modulated states.

Key words Modulated structure · Order-disorder · β-eucryptite · Transmission electron microscopy · electron diffraction

H. Xu (✉)[1] · P.J. Heaney[2]
Department of Geosciences and Princeton Materials Institute, Princeton University, Princeton, New Jersey 08544, USA

H. Böhm
Institut für Geowissenschaften, Johannes Gutenberg Universität, D-55099 Mainz, Germany

Present address:
[1] Thermochemistry Facility,
Department of Chemical Engineering and Materials Science, University of California at Davis, Davis, California 95616, USA
e-mail: hxu@ucdavis.edu
[2] Department of Geosciences, The Pennsylvania State University, University Park, Pennsylvania 16802, USA

Introduction

Beta-eucryptite ($LiAlSiO_4$) is a stuffed derivative of β-quartz in which half the tetrahedral Si^{4+} cations are replaced by Al^{3+} and the charge is balanced by the incorporation of Li^+ into the main channels of the structure (Buerger 1954; Palmer 1994). This material is of considerable interest because of its one-dimensional superionic conductivity due to Li^+ diffusion in the structural channels (Alpen et al. 1977; Nagel and Böhm 1982). Hence, it can potentially be used as a solid electrolyte in Li-based electric batteries. In addition, β-eucryptite exhibits near-zero thermal expansion coefficients (Schulz 1974; Haussühl et al. 1984; Lichtenstein et al. 1998; Xu et al. 1999). As a result, it has served as a component of high-temperature glass-ceramic products (Beall 1994).

A number of crystal structure analyses of β-eucryptite (Winkler 1948; Buerger 1954; Tscherry et al. 1972a, b; Pillars and Peacor 1973; Guth and Heger 1979) have revealed that its translational periodicity is doubled along **c** and **a** relative to the β-quartz structure. This superstructure results from ordering of Al and Si cations in alternate layers normal to **c** with concomitant ordering of Li ions within two distinct channels (Fig. 1A, B). As a result, in addition to the primary β-quartz-like reflections (h, k, l = even), two classes of superlattice reflections are produced: (1) *c*-reflections: h, k = even; l = odd, corresponding to Al/Si order; and (2) *a*-reflections: h, k = odd or $h+k$ = odd; l = odd, reflecting Li positional ordering (Tscherry and Schulz 1972; Müller and Schulz 1976).

High-temperature X-ray and neutron diffraction experiments (Tscherry and Laves 1970; Schulz and Tscherry 1972b; Pillars and Peacor 1973; Guth and Heger 1979) show that *a*-superlattice reflections become weaker and more diffuse with increasing temperature and disappear at some temperature between 673 K and 755 K. The large range of the reported critical temperatures (T_c) is due not only to different synthesis conditions of the samples but also to variations in the

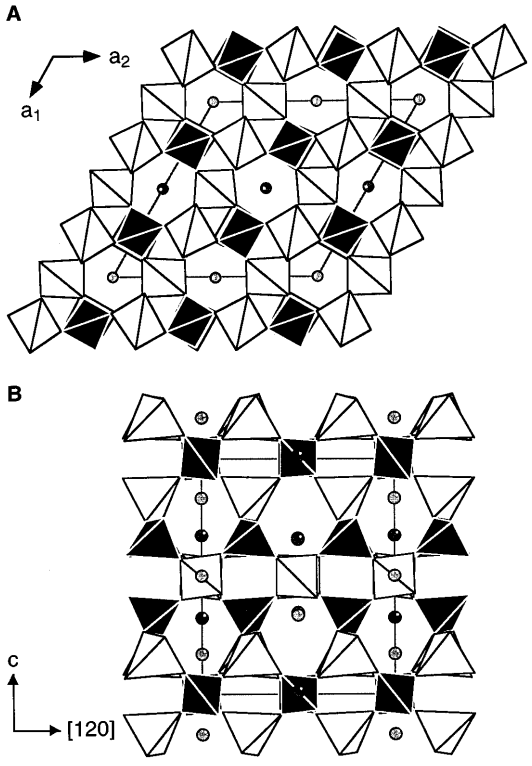

Fig. 1A, B The structure of β-eucryptite projected down **A** the **c**-axis and **B** **a**-axis. *Spheres* represent Li ions; Si- and Al-tetrahedra are plotted in *black* and *white*, respectively. *Light lines* outline the unit cell. Structural data are from Pillars and Peacor (1973)

resolution of the analytical techniques used, because the *a*-reflections are generally very weak and hence difficult to detect. In addition, recent neutron scattering (Press et al. 1980) and X-ray (Böhm 1983) diffraction studies have revealed an incommensurate structure that bridges the boundary between the low-temperature ordered phase and the high-temperature disordered phase. This intermediate phase can occur over a temperature range of 60 K (703–763 K), and Press et al. (1980) assert that it can coexist with the low-temperature phase from 703 to 755.5 K. These authors argue for two transitions in β-eucryptite. The first purportedly occurs at 763 K and represents the inversion from the high-temperature modification to the modulated phase, and the second at 755.5 K and is associated with the appearance of the *a*-superlattice reflections.

Although most workers interpret the transition in β-eucryptite in terms of Li^+ positional disordering at elevated temperatures, Schulz and Tscherry (1972a, b) argue that structural elements in the low-temperature phase are α-quartz-like, such that the Al/Si framework undergoes a displacive transition accompanying the change in Li order-disorder at ~673 K. The discovery of the intermediate phase has led other researchers to postulate that the transition in β-eucryptite involves a distortion of the Al/Si framework (Press et al. 1980; Böhm 1983) by analogy with the incommensurate phase that occurs over a temperature range of 1.3 K between α- and β-quartz, composed of ordered triangular prismatic Dauphiné microtwins (Van Tendeloo et al. 1976). Correspondingly, the Al/Si framework of β-eucryptite might distort in a manner that is analogous to the α-β quartz transformation at the transition temperature (Schulz and Tscherry 1972a, b; Böhm 1983).

As is well known, the transition from β- to α-quartz results from a distortion of the tetrahedral chains that lowers the symmetry from hexagonal to trigonal (see reviews by Heaney and Veblen 1991; Heaney 1994). The distortion is effected by the tilting of tetrahedra in one of two possible orientations, which results in two distinct Dauphiné twins. These twins are related by the twofold rotation parallel to the **c**-axis that is contained within the sixfold screw axis of β-quartz ($P6_422$ or $P6_222$) but absent in α-quartz ($P3_121$ or $P3_221$). If β-eucryptite undergoes a β-to-α-quartz-like transition, then Dauphiné macrotwins should characterize the low-temperature phase, and the apparent hexagonal symmetry of β-eucryptite must arise from an averaging of the merohedral twins.

In fact, a single-crystal neutron diffraction study by Guth and Heger (1979) suggests that β-eucryptite may deviate from hexagonal symmetry, and merohedral twins presumably occur within the low-temperature phase. The evidence for this speculation is the presence of weak reflections of the type $00l$, $l \neq 3n$, which are forbidden by the space group $P6_222$ or $P6_422$. However, these reflections are forbidden in a trigonal α-quartz-like structure as well. Thus, Guth and Heger's (1979) results suggest that at room temperature, β-eucryptite must have an even lower symmetry, presumably orthorhombic ($C222$) or monoclinic ($P112$). Moreover, given that the thermal parameters of Si, Al and O in β-eucryptite are similar to those in quartz, the authors exclude the possibility that the lower symmetry is due to a statistical superposition of distorted Si- and Al-tetrahedra. Rather, they attribute the extra reflections to small changes of the Li distribution parallel to **c**. Similarly, based on X-ray diffraction studies of their samples that were synthesized by glass-annealing, Behruzi and Hahn (1971) claim that besides the hexagonal form, β-eucryptite can also crystallize in monoclinic or triclinic distortions of the β-quartz structure.

In addition to doubled **c**- and **a**-axes with respect to β-quartz, β-eucryptite may adopt a variety of modulated structures with superperiodicities along **a**. For instance, in their ionic conductivity studies of β-eucryptite, Nagel and Böhm (1982) describe a phase in which *a*-reflections are absent, but pairs of satellite reflections straddle the absent *a*-reflections. Compounds with this modulation display considerably higher conductivity perpendicular to the **c**-axis than those without this superstructure. Electron diffraction analyses of the β-eucryptites annealed at 1523 K for various times reveal that the structural modulation parallel to **a** undergoes a sequence of changes with increasing annealing time: streaked *a*-reflections; *a*-reflections surrounded by a pair of satellites; and pairs of satellites with *a*-reflections absent (Krause and Böhm 1982). However, the structural

characteristics of these modulated phases and their formation mechanisms remain largely unclear.

In light of the questions surrounding the transformation in β-eucryptite, we concluded that direct observation by in-situ transmission electron microscopy (TEM) at the transition might provide some critical insights into the reaction mechanism. This technique has proved a powerful tool for investigating displacive phase transitions and fast order-disorder reactions (Nord 1992). While dark-field TEM can readily be used to image transformation-induced domains (twins or antiphase domains (APDs)), conventional selected-area electron diffraction (SAED) and convergent-beam electron diffraction (CBED) provide corresponding structural information.

Sample and experimental techniques

The β-eucryptite single crystal used in this study was grown from a LiF/AlF_3 flux. The detailed growth procedures have been described elsewhere (Schönherr and Schedler 1977). The sample is a transparent, ~1 cm, pyramidic crystal. Thin sections were cut normal to the morphological **a**- and **c**-axes and parallel to the (100) plane and thinned further by Ar ion milling. Foils supported by Cu grids of 3-mm diameter were then coated lightly with amorphous C.

TEM observations were conducted using a Philips CM-20 and a Philips FEG CM-200 microscope both equipped with a supertwin objective lens and operated at 200 keV. Cooling experiments were carried out with a Gatan model 636 double-tilt cooling holder with a low-temperature limit of ~100 K. Specimens were cooled by liquid nitrogen in a vacuum-insulated reservoir. Intermediate temperatures between 100 K and 403 K were achieved by controlled heating of a copper heat-transfer rod between the specimen and the N_2 reservoir. Cooling the specimens not only eliminates contamination caused by residual hydrocarbon vapor inside the microscope but also reduces electron beam heating, which is especially critical when CBED experiments are performed.

Heating experiments were performed with a Gatan model 652 double-tilt heating holder. Specimens were heated by an annular tantalum furnace, which warmed in response to an increase in electrical current through a molybdenum strip heater. Furnace temperatures were registered by a Pt-13% Rh thermocouple spot welded to the furnace body. However, because of the poor thermal conductivity between the furnace and the specimens, the actual temperature of the specimens was lower than the furnace temperatures. Our investigations of quartz and anorthite using the same holder indicate that the difference in temperature between the furnace and the specimen ranges from 15 to 95 K (Xu and Heaney 1997).

Results and analysis

Symmetry of β-eucryptite

In addition to the phase transition at ~723 K that produces the *a*-reflections, β-eucryptite very likely experiences an Al/Si disordering transformation that involves a doubling of its lattice constant *c* at higher temperature, as occurs in anorthite (e.g., Heuer and Nord 1976; Carpenter 1988). As a result, the multiple transitions that characterize β-eucryptite give rise to the *a*- and *c*-superlattice reflections. Figure 2A is an SAED pattern obtained with the electron beam parallel to the [010] zone axis of β-eucryptite. Both the quartz-like main reflections and the *c*- and *a*-superlattice reflections are evident in this pattern. Primary reflections are strongest, *a*-reflections weakest, and *c*-reflections intermediate in intensity. These intensity relationships are consistent with the structure factor amplitudes calculated using the hexagonal structure of Tscherry et al. (1972b).

As would be expected, a [001] zone-axis SAED pattern of β-eucryptite more clearly shows its hexagonal symmetry (Fig. 2B). In addition to the strong substructure reflections (e.g., 200 and 400) characteristic of a phase with the quartz structure, the pattern also has weak *a*-superstructure reflections (e.g., 100 and 010). Although the *a*-reflections are relatively faint in this pattern, they exhibit much stronger intensities along the first-order Laue zone (FOLZ) axis (Fig. 2C), which also is in agreement with the hexagonal model.

However, additional weak reflections of the type 00*l*, $l \neq 3n$, which are forbidden by the space group $P6_222$ or $P6_422$, also are present in Fig. 2A. In their neutron diffraction study of β-eucryptite, Guth and Heger (1979) also noted the existence of these reflections, and they interpreted them as evidence for lower symmetry in their sample (orthorhombic or monoclinic). The authors further postulated that the average pseudo-hexagonal structure may result from merohedral twinning. However, our attempts to image possible merohedral twins by dark-field imaging with 00*l* ($l \neq 3n$) reflections failed

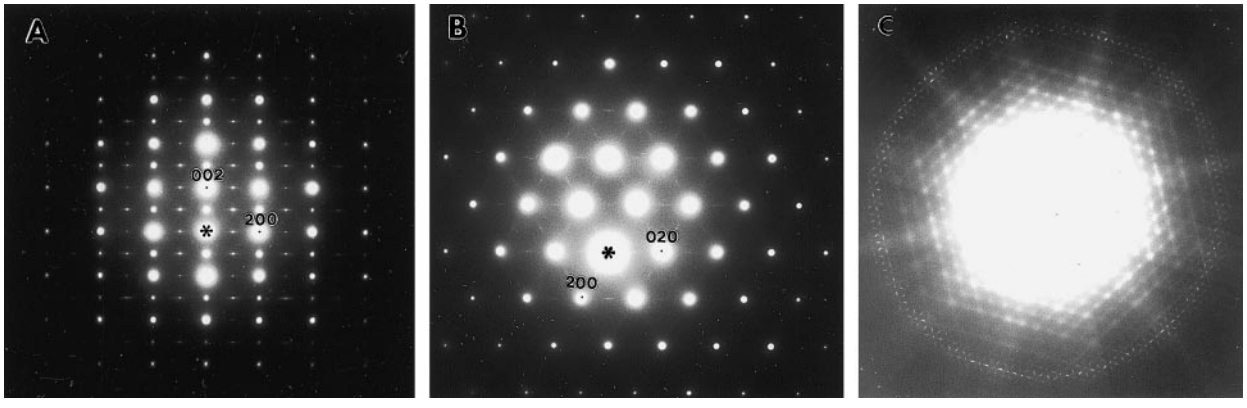

Fig. 2A–C SAED patterns of β-eucryptite with the electron beam parallel to **A** [010] and **B, C** [001]

to detect any textural features. Therefore, we conclude that the extra spots in our SAED patterns are due to dynamical diffraction of electrons, as commonly occurs. Because multiple scattering of neutrons is negligible, the presence of the 00*l* ($l \neq 3n$) reflections observed by Guth and Heger (1979) may be related to the synthesis conditions of the sample used. As noted by Nagel and Böhm (1982) and Krause and Böhm (1982), β-eucryptite can easily adopt different structural states with respect to Li ion distributions when the specimens are prepared or heat-treated at different conditions.

In light of the possible occurrence of Dauphiné twins in β-eucryptite, we also performed careful dark-field imaging with appropriate reflections, such as 601. In an SAED pattern taken across Dauphiné twin boundaries, the *hkl* spot of one twin configuration will be superimposed on $hk\bar{l}$ of the other. By forming a dark-field image from a diffracted beam with structure factors F(*hkl*) and F($hk\bar{l}$) that differ markedly, adjacent twin domains will exhibit strong amplitude contrast (McLaren and Phakey 1969). However, no such domains were observed, even at relatively high magnifications (Fig. 3).

CBED offers the possibility of providing symmetry information from a region as small as a few nanometers. Under a convergent electron beam, however, β-eucryptite foils tend to amorphize within a few seconds, even with a small spot size and at very low temperature. Because there was not enough time to orient the specimen and to record the pattern, we first obtained a well-oriented pattern from one region, and then we slightly moved the specimen to another area to record a pattern. Two ZOLZ (zero-order Laue zone) CBED patterns along [001] and [010] are shown in Fig. 4A and B, respectively, which were taken with an electron beam size of ~50 nm at ~100 K. Since β-eucryptite does not undergo a structural transition between 20 and 300 K as shown by our synchrotron X-ray diffraction work (Xu et al. 1999), these patterns can be used to determine its symmetry at room temperature. The [001] pattern displays a symmetry of 6 *mm*, and the [010] pattern a symmetry of 2 *mm*. According to the CBED pattern symmetry and the zone-axis symmetry tables (Williams and Carter 1996), the possible point groups are 622, 6 *mm* and 6/ *mmm*. Since previous structure analyses (e.g., Tscherry et al. 1972a, b; Pillars and Peacor 1973) have not revealed the existence of mirror or glide planes, the choices of 6 *mm* and 6/ *mmm* can be eliminated. Therefore, the point group is uniquely determined as 622, which is consistent with the space group $P6_222$ or $P6_422$.

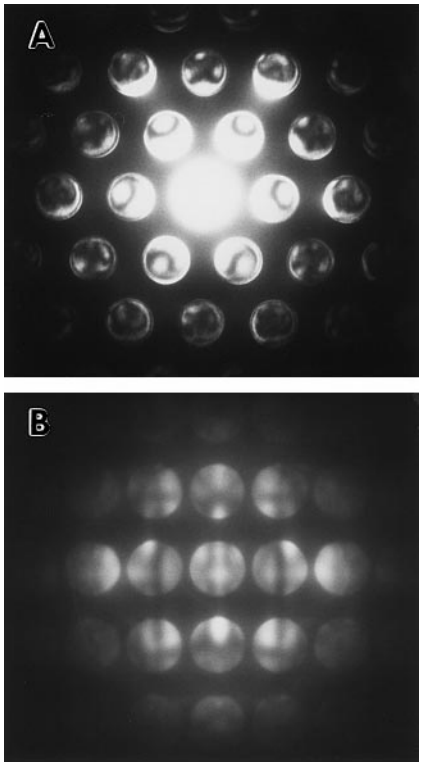

Fig. 4A, B ZOLZ CBED patterns of β-eucryptite with zone axes **A** [001] and **B** [010]. Note pattern **A** displays a sixfold rotation along the **c**-axis and six mirror planes coincident with (100), (010), (110), ($1\bar{1}0$), ($1\bar{2}0$) and ($2\bar{1}0$). In **B**, there is a twofold rotation along the (010) and two mirror planes parallel to (100) and (001)

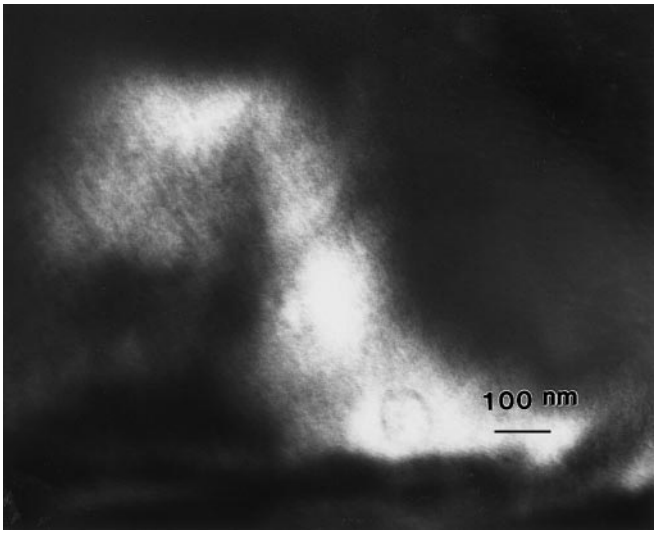

Fig. 3 A dark-field image using the 601 reflection, revealing no evidence for Dauphiné twins as appeared in α-quartz

However, two points concerning our CBED analysis should be stressed here. First, as commonly occurs in CBED patterns, weak disks of superlattice reflections such as the *a*- and *c*-reflections of β-eucryptite are easily hidden in the inelastic diffuse background. Thus, the structural symmetry revealed by our CBED patterns corresponds only to the quartz-like substructure without reflecting the superstructure. Second, if the merohedral domains with lower symmetry occur at the unit-cell scale, the CBED patterns actually show the symmetry averaged over many domains rather than the symmetry of a single domain. In this case, a high-resolution TEM determination (with a CCD camera for recording) might be desirable.

Table 1 Selected structure factors for ordered β-eucryptite ($P6_222$)[a]

(*hkl*)	$\lvert F_o \rvert$
103	21.6
113	25.2
115	22.4
423	21.5
433	25.5

[a] Calculated by the program LAZY; the atomic coordinates and lattice constants used are from Guth and Heger (1979)

Imaging the *a*-antiphase domains

If β-eucryptite is strictly a structural derivative of β-quartz, the down-temperature inversion of the Li-disordered to the Li-ordered phase involves a doubling of the lattice parameter *a* while the space group $P6_422$ or $P6_222$ is conserved. As described by Müller and Schulz (1976), such a transition produces APDs that are related by the lost translation vector 1/2 **a**. These domains can be imaged by dark-field TEM with *a*-reflections, and they are called *a*-APDs to distinguish them from the APDs that arise from the Al/Si ordering. The intensities of *a*-reflections vary, and the more intense ones, such as 113 (Table 1), provide superior contrast (Fig. 5A, B).

It is apparent from Fig. 5A, B that the *a*-antiphase domain boundaries (*a*-APBs) show a strong preferred orientation along the **c**-axis within the same crystal. Moreover, the *a*-APBs can be either flat planar (Fig. 5B) or undulatory (Fig. 5A), and the domain widths can be highly variable, ranging from 10 to 250 nm.

The tendency of the APBs to orient themselves parallel to **c** can be attributed to their relationship to Li ions along the channels parallel to **c**. As mentioned earlier, in the low-temperature ordered structure, two kinds of channels (denoted as A and B) are distinguished based on their Li distributions (Fig. 6A). The Li(1) cations

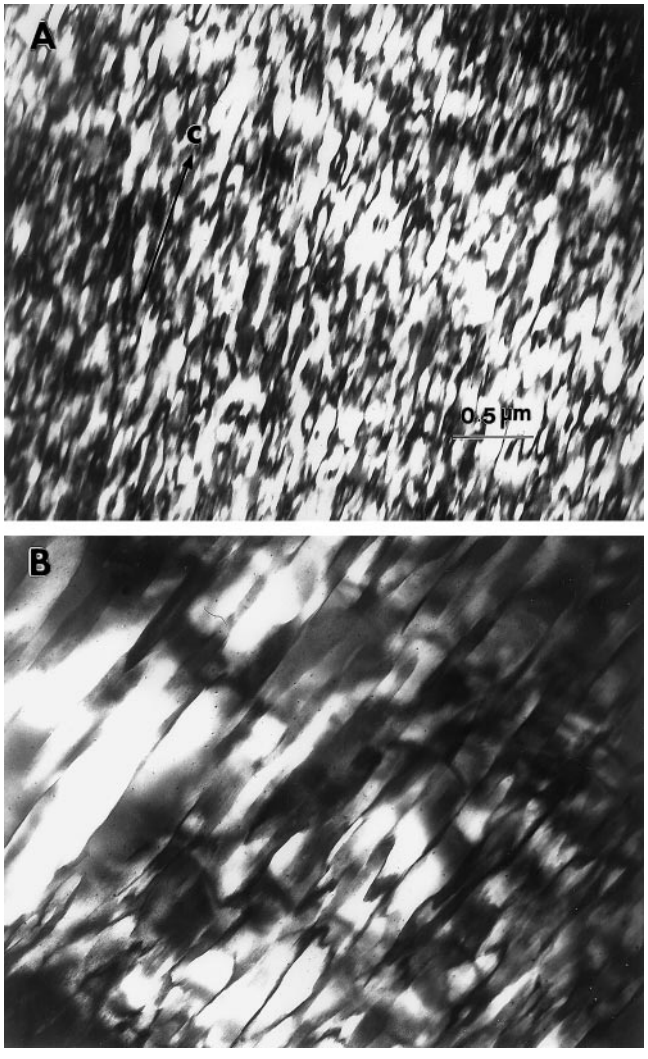

Fig. 5A, B Dark-field images of *a*-APDs using the 113 diffracted beam. **A** and **B** were taken from two different regions of a single specimen

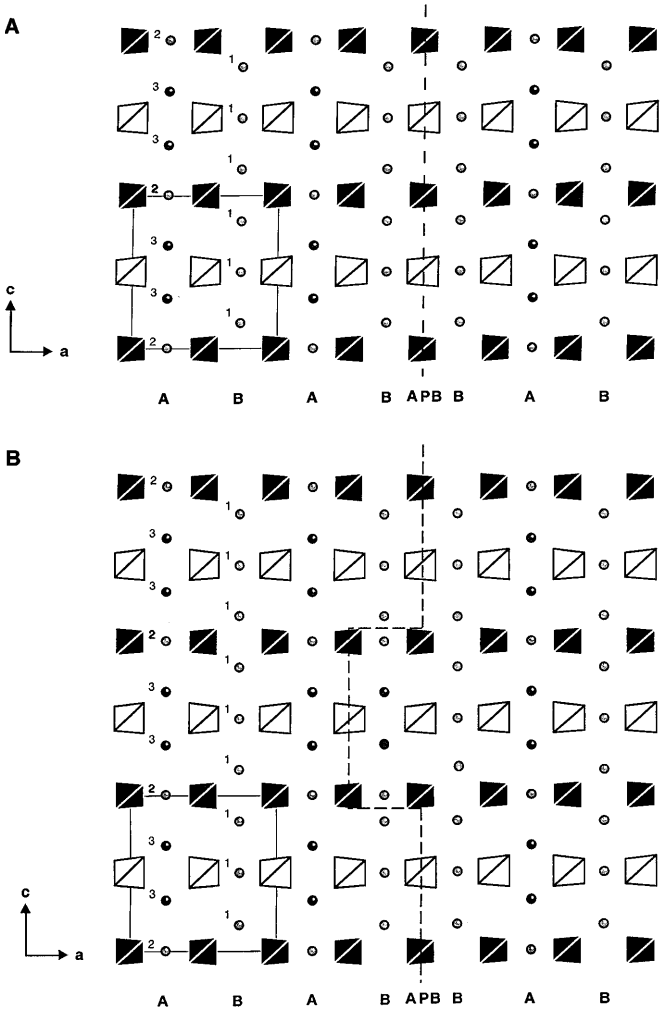

Fig. 6 A A schematic structural model of the APB resulting from Li ordering. For clarity, only atoms with their *y* coordinates ranging from −0.3 to 0.3 are projected. *Spheres* represent Li ions; Si- and Al-tetrahedra are shown in *black* and *white*, respectively; **B** A structural model of the wavy APBs shown in Fig. 5A

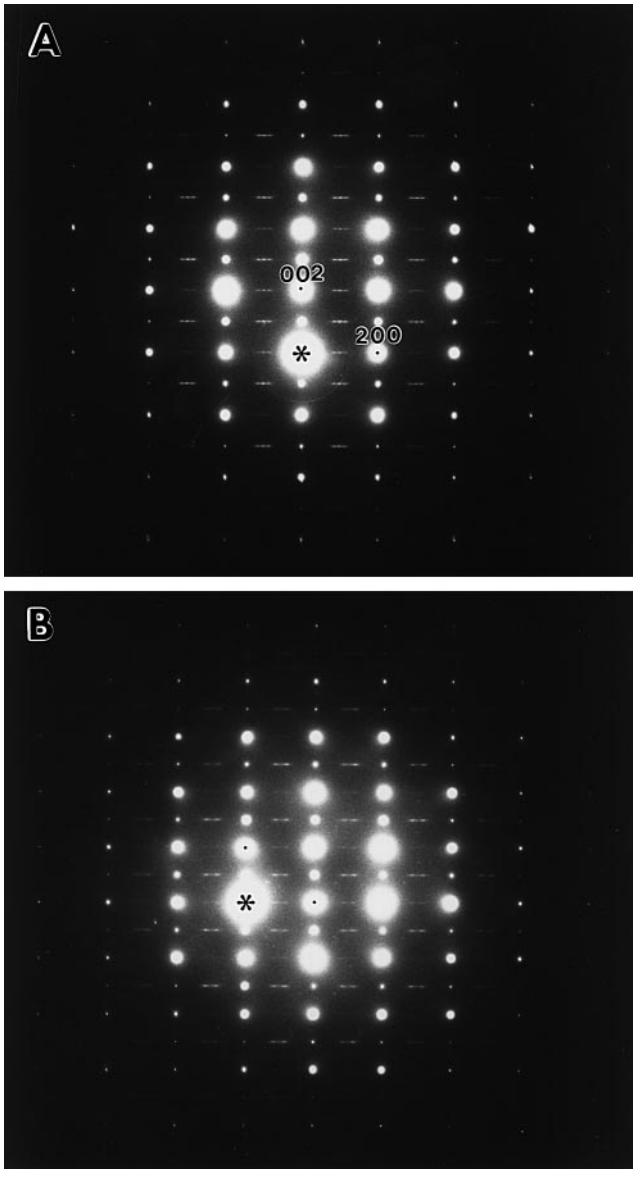

Fig. 7A, B SAED patterns of two modulated structures with zone axis [010]

reside only in the B channels within the layer of Al-tetrahedra. The remaining two sets of cations, Li(2) and Li(3), are situated within the A channels and are surrounded by Si-tetrahedra. Vacant and occupied tetrahedral sites for Li alternate along any channel axis, and the alternation sequence for neighboring channels is antisympathetic in the ideal ordered structure. An APB is generated by the loss of either an A or a B channel in the ABAB... ... repeating sequence (Fig. 6A). If Li occupancy in adjacent channels occurs with long range order along **c**, straight APBs are produced (Fig. 6A). Otherwise, a zig-zig type of APB at the atomic scale results in a wavy character (Fig. 6B). Because of the relatively strong repulsion between two adjacent Li cations (1/6 *c* instead of 1/3 *c*) at the segments parallel to **a**, the wavy APB is expected to be energetically less favorable.

Structural modulations

Nagel and Böhm (1982) note that the Li distribution of β-eucryptite may adopt different patterns, depending on growth conditions of the crystals. As a result, a variety of modulations have been observed for the samples crystallized from glass at different temperatures (Krause and Böhm 1982). Our own electron diffraction analysis shows that different kinds of modulated structures can also coexist within a single sample. In addition to the ordered β-eucryptite region, we found two types of modulations that exhibit different SAED patterns when the electron beam is parallel to the **a**-axis. The main differences between these patterns lie in the characteristics of the *a*-reflections.

Figure 7A is an SAED pattern of one of the modulated structures. The pattern shows *a*-reflections that are each surrounded by a pair of satellite spots along **a***. The distribution of the satellites indicates that the modulated structure is two-dimensional (two **a**-axes for hexagonal symmetry), and from their spacing the modulation period is calculated as $6.5d_{100}$ (≅ 59 Å) and hence the structure is incommensurate. A dark-field image obtained with an *a*-reflection (e.g., 113) and its satellites reveals ∼60 Å modulation fringes that are parallel to the (100) plane. These fringes are also parallel to *a*-APBs and they can more clearly be seen within individual *a*-APDs (Fig. 8). Figure 9 illustrates a schematic structural model for this modulated structure. The relationship between the supercell and the eucryptite subcell is as follows: $\mathbf{a}_{sup} \cong 6.5\mathbf{a}_{sub}$, $\mathbf{c}_{sup} \cong \mathbf{c}_{sub}$ (where "sup" and "sub" refer to supercell and subcell, respectively). From this geometry, the modulated

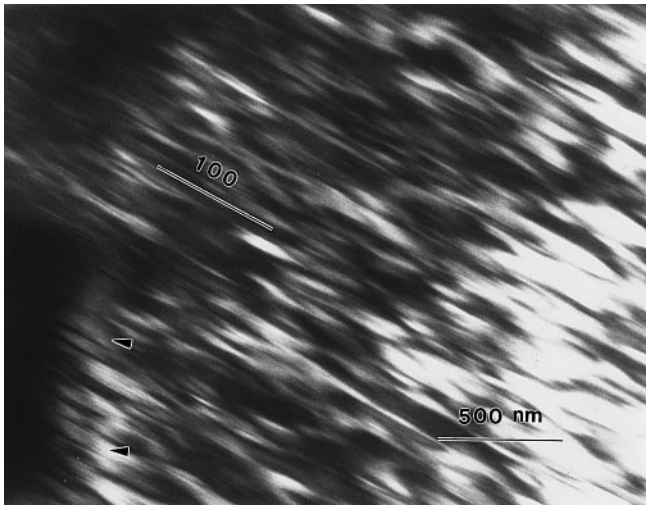

Fig. 8 A dark-field micrograph of the modulated structure using the 113 diffracted beam. Note modulation fringes can be more clearly seen within *a*-APDs (*arrows*)

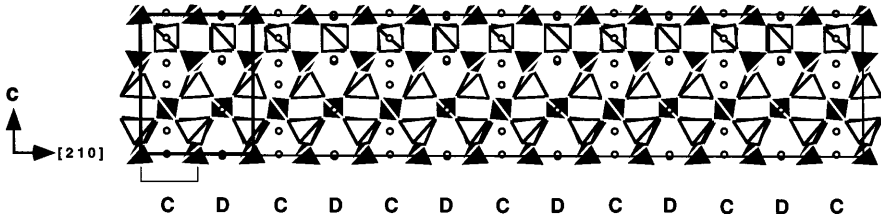

Fig. 9 A schematic structural model showing the relationship between the supercell and the subcell of the modulated structure

structure can be thought of as superperiodic stacking parallel to (100) of two structural units (denoted as C and D) with different Li configurations, and domains are related by a translation of 1/2 $\mathbf{a}_{sub}$ across antiphase boundaries. The streaking along **a*** suggests irregularities in modulation periodicity.

Figure 7B is a [010] zone-axis SAED pattern of another modulated structure, which is more common within the specimen. In contrast to Fig. 7A, *a*-reflections are absent but their satellites remain. This behavior probably indicates that the superstructure cell is either face- or body-centered. It is also possible that a translation-symmetry element (glide plane or screw axis) is present in the structure. As the intensities of the satellites were too weak, attempts to image the domain structure that produced them failed to reveal any textural features. In addition, since the *a*-reflections were absent in these regions, even the APBs themselves could not be imaged at the dark-field mode.

Interestingly, the modulated structures described are similar to those observed in β-eucryptite at 703–763 K by Press et al. (1980). In their high-temperature neutron scattering study, Press et al. (1980) noted that two satellite peaks appeared about an *a*-reflection when the temperature was between 703 and 755.5 K. But as the specimen was heated above 755.5 K, the *a*-reflection peak disappeared, while satellite peaks still could be seen up to 763 K, although they became much more diffuse. The authors interpreted the scattering profile between 703 and 755.5 K as representing the coexistence of the ordered β-eucryptite superstructure and an intermediate incommensurate phase, whereas the profile between

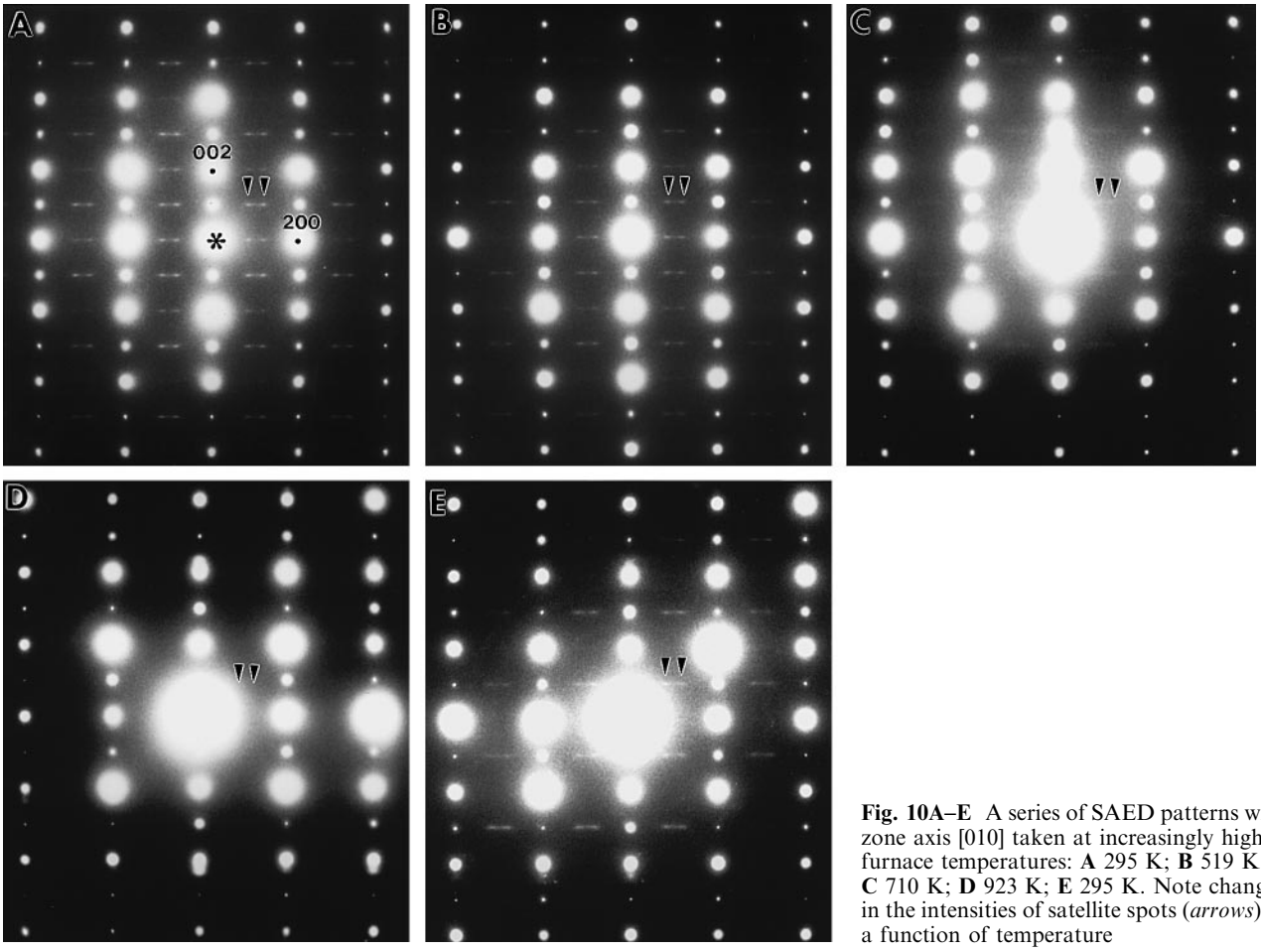

Fig. 10A–E A series of SAED patterns with zone axis [010] taken at increasingly higher furnace temperatures: **A** 295 K; **B** 519 K; **C** 710 K; **D** 923 K; **E** 295 K. Note changes in the intensities of satellite spots (*arrows*) as a function of temperature

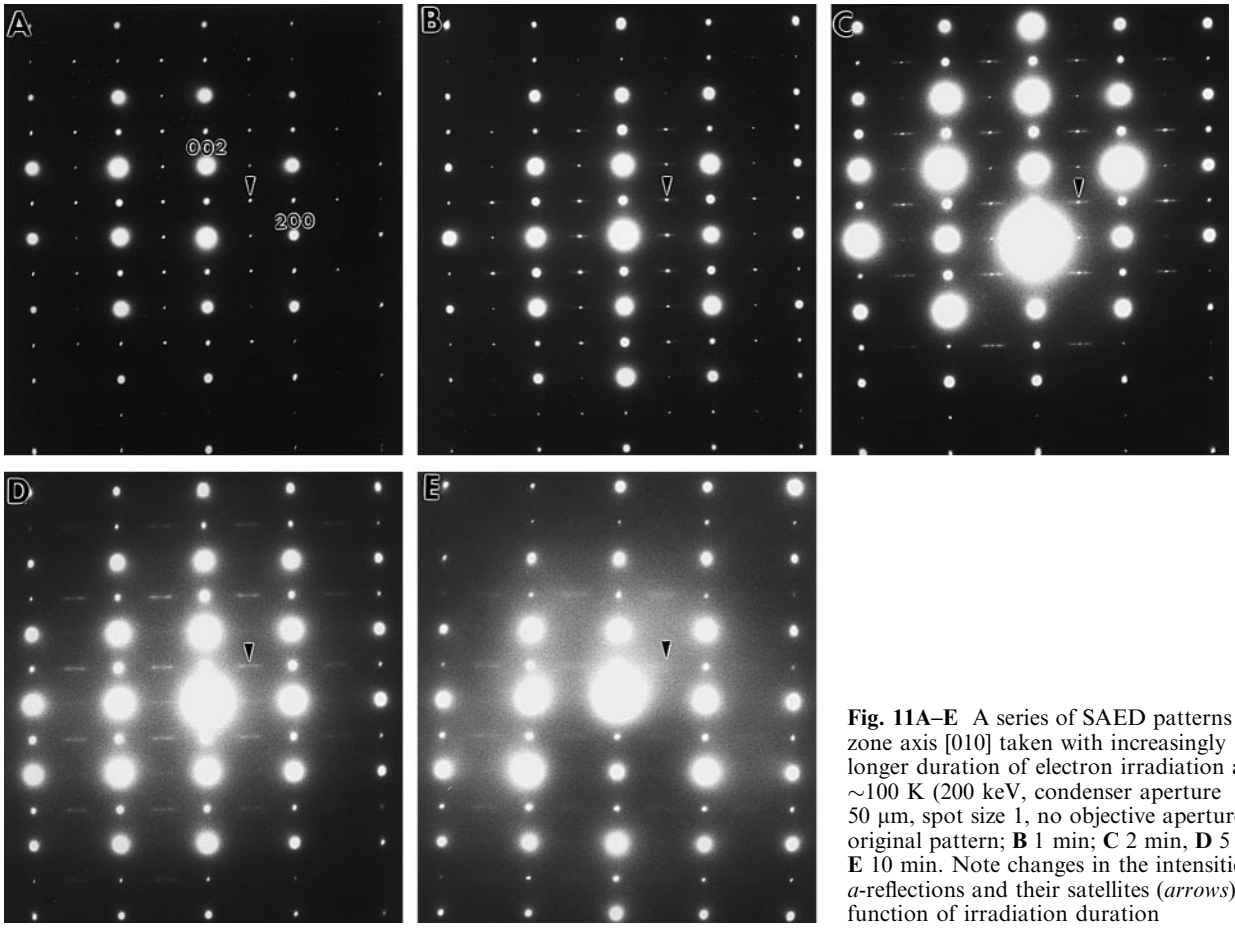

Fig. 11A–E A series of SAED patterns with zone axis [010] taken with increasingly longer duration of electron irradiation at ~100 K (200 keV, condenser aperture 50 μm, spot size 1, no objective aperture): **A** original pattern; **B** 1 min; **C** 2 min, **D** 5 min; **E** 10 min. Note changes in the intensities of *a*-reflections and their satellites (*arrows*) as a function of irradiation duration

755.5 and 763 K was attributed only to the intermediate structure. In light of the similarity in diffraction profiles, it is possible that the intermediate phase described by Press et al. (1980) can be quenched and is identical to the modulated structure that we observed at room temperature.

In situ heating experiments

To further explore the formation mechanism of the modulated structures, we performed in-situ heating experiments while observing the specimen in the TEM. Figure 10A–E is a sequence of SAED patterns of the most common modulated structure (Fig. 7B) along the **a**-axis as a function of temperature. At room temperature, the satellites were very distinct, although they exhibited strong streaking along **a***. With increasing temperature, the satellites became perceptibly weaker until they no longer could be observed when the furnace temperature was increased to ~923 K. Upon cooling to room temperature, the satellites reappeared at their previous positions. Both primary reflections and *c*-reflections persisted at all temperatures.

The constant presence of *c*-reflections during our in situ heating experiments indicates that there were no changes in the state of Al/Si order at these temperatures. Although no kinetic studies have been performed on Al/Si ordering in β-eucryptite, intensive investigations of other aluminosilicates such as anorthite (e.g., Carpenter et al. 1990) suggest that Al/Si diffusion should be extremely sluggish under the conditions of our experiments. In addition, as described earlier, the absence of merohedral twins eliminates the possibility that the phase transition could arise from a displacive distortion of the Al/Si framework. These considerations support our interpretation that the reversible transition behavior demonstrated in our experiments is due to positional disordering of Li ions along the main structural channels.

Electron irradiation

As noted by Müller and Schulz (1976), *a*-reflections become increasingly diffuse under electron beam irradiation. As a result, dark-field imaging of *a*-APBs becomes more and more difficult as the *a*-reflections weaken. This behavior can be ascribed to the high mobility of Li ions within the structural channels.

Our diffraction experiments revealed that the electron beam can transform the irradiated region from the ideal β-eucryptite structure with *a*-reflections to the modulated structure that is characterized by pairs of satellites

about the *a*-reflections and then to the modulation in which *a*-reflections are absent but satellites remain. Figure 11A–E is a series of [010] zone-axis SAED patterns taken after the specimen region had been irradiated for 0, 1, 2, 5, and 10 mins at ~100 K under the same illumination conditions (200 keV, condenser aperture 50 μm, spot size 1, no objective aperture, irradiated area ~16 μm^2). The corresponding dark-field images using the 113 reflection are shown in Fig. 12A–D. Since both SAED patterns and dark-field images were taken with defocused electron beams, the effect of the beam irradiation during the recording is probably negligible. Before the irradiation experiments were begun, the *a*-reflections were sharp (Fig. 11A) and *a*-APBs were clear (Fig. 12A). With increasing duration of irradiation, the *a*-reflections changed in the following fashion: first, the *a*-reflections exhibited slight streaking along **a*** (Fig. 11B); next, a pair of satellites appeared about each of the *a*-reflections (Fig. 11C); then, the *a*-reflections became unobservable (Fig. 11D); and lastly the satellites became barely observable (Fig. 11E). Correspondingly, *a*-APDs first showed no discernible changes but then grew smaller and more diffuse (Fig. 12B, C) until they no longer could be observed in Fig. 12D.

It is well known that electron beam irradiation can increase the specimen temperature through the inelastic collisions of electrons with the specimen, especially for materials with low thermal conductivity (Williams and Carter 1996). This raises the possibility that beam heating may induce migration of Li ions along the channels, thereby disordering the Li, so that the *a*-reflections would grow more diffuse. By analogy with other Li-based one-dimensional superionic conductors, such as $Li_2B_4O_7$, the disordering of Li in β-eucryptite might start well below its critical temperature (M. Zhang personal communication). Infrared spectroscopic experiments suggest that the lowest temperature for the movement of Li ions in β-eucryptite is ~500 K (Zhang et al. in preparation), and this temperature can be achieved by electron beam heating. However, it is very difficult to determine the

Fig. 12A–D A series of dark-field images (**g** = 113) of the same area with increasing electron irradiation at ~100 K. **A–D** correspond to the SAED patterns A(B), C, D and E in Fig. 11, respectively. There are no discernible changes in APBs corresponding to Fig. 11A, B

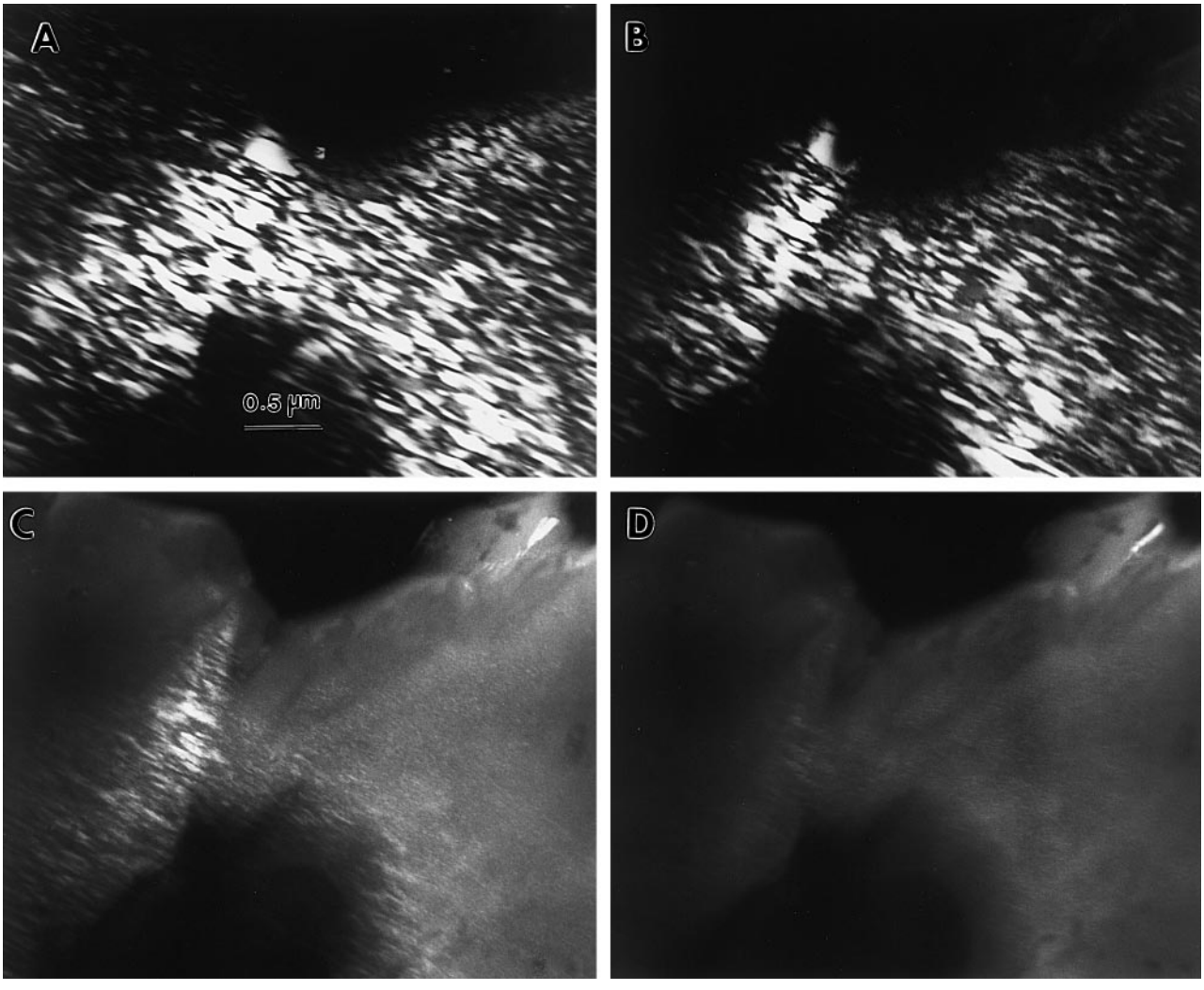

specimen temperature under electron beam irradiation, for the temperature is affected by many variables such as specimen thickness and beam size. Calculations by Hobbs (1979) show that the increase in temperature due to beam heating generally ranges from tens to hundreds of degrees for ceramic materials when the electron source of a TEM is thermionic.

Nevertheless, our investigations with the same microscope of another aluminosilicate, anorthite ($CaAl_2Si_2O_8$), demonstrate that its $P\bar{1}$-$I\bar{1}$ transition at ~514 K was not induced by electron beam heating under the conditions that characterized our investigations (Xu and Heaney 1997). Therefore, we believe that beam heating was not the major factor responsible for the phase transition behavior induced by electron irradiation, particularly because our irradiation experiments were performed at ~100 K. Rather, given the very small activation energy of ionic conductivity of β-eucryptite (0.79 ± 0.02 eV, Nagel and Böhm 1982), we propose that the electron beam activated Li migration along the channels, allowing a series of phase transitions involving Li redistribution to occur.

In addition, the decrease in size of the *a*-APDs with increasing electron irradiation is strongly reminiscent of domain behavior at the α-β quartz and the $P\bar{1}$-$I\bar{1}$ anorthite transitions (Van Tendeloo et al. 1976, 1989). Like β-quartz and $I\bar{1}$ anorthite, disordered β-eucryptite induced by electron irradiation may be a statistical-dynamic average of small *a*-APDs. If electron irradiation and heating exert similar effects on Li order-disorder, this observation is consistent with the dynamic character of Li above the transition temperature: Li ions do not statically occupy only one of the two sets of tetrahedral positions that alternate along **c** (Schulz and Tscherry 1972a, b). Rather, they are dynamically distributed over all possible sites within the channels.

Conclusions

Because of the interactive ordering of Li ions in adjacent channels, in addition to the superstructure whose lattice constant *a* is doubled relative to β-quartz, β-eucryptite adopts a variety of modulated structures parallel to the **a**-axes. The coexistence of these structures within the same crystal suggests that the energy differences between the various configurations are quite small. Upon heating or prolonged electron irradiation, however, all the structures can transform to the modification with a disordered Li distribution either directly or through an intermediate phase(s). In particular, the ideal β-eucryptite structure undergoes a series of transitions with increasing temperature or irradiation: ordered β-eucryptite → incommensurate phase with a 6.5 **a** modulation → incommensurate structure with the presence of a centering or a translation-symmetry → disordered β-eucryptite. These transitions arise from positional order-disorder of Li ions along the structural channels without distortions in the Al/Si framework.

Acknowledgements This work was supported by the NSF grants EAR-9418031 and EAR-9706143 (to P.J.H.) and the 1996 and 1997 ICDD crystallography scholarships (to H.X.). Electron microscopy was performed at the General Motors Electron Microbeam Facility of the Princeton Materials Institute. We would like to acknowledge Dr. M.A. Carpenter and an anonymous reviewer for their helpful comments and Dr. D.L. Kohlstedt for his editorial assistance.

References

Alpen U, Schulz H, Talat GH, Böhm H (1977) One-dimensional cooperative Li-diffusion in β-eucryptite. Solid State Commun 23: 911–914

Beall GH (1994) Industrial applications of silica. In: Heaney PJ, Prewitt CT, Gibbs GV (eds) Silica. Reviews in Mineralogy, vol 29, Mineralogical Society of America, Washington, DC, pp 468–505

Behruzi M, Hahn T (1971) Hoch-$LiAlSiO_4$ und verwandte phasen in system $LiAlSiO_4$-$LiGaSiO_4$-$LiAlGeO_4$-$LiGaGeO_4$. Z Kristallogr 133: 405–421

Böhm H (1983) Modulated structures at phase transitions. Am Mineral 68: 11–17

Buerger MJ (1954) The stuffed derivatives of the silica structures. Am Mineral 39: 600–614

Carpenter MA (1988) Thermochemistry of aluminum/silicon ordering in feldspar minerals. In: Salje EKH (ed) Physical properties and thermodynamic behavior of minerals. NATO ASI C, 225, Reidel, Dordrecht, pp 265–323

Carpenter MA, Angel RJ, Finger LW (1990) Calibration of Al/Si order variations in anorthite. Contrib Mineral Petrol 104: 471–480

Guth H, Heger G (1979) Temperature dependence of the crystal structure of the one-dimensional Li^+-conductor β-eucryptite ($LiAlSiO_4$). In: Vashista P, Mundy JN and Shenoy GK (eds) Fast ion transport in solids. Elsevier, North Holland, pp 499–502

Haussühl S, Nagel W, Böhm H (1984) Elastic and thermoelastic constants of hexagonal β-$LiAlSiO_4$. Z Kristallogr 169: 299–303

Heaney PJ (1994) Structure and chemistry of the low-pressure silica polymorphs. In: Heaney PJ, Prewitt CT, Gibbs GV (eds), Silica. Reviews in Mineralogy, vol 29. Mineralogical Society of America, Washington, DC, pp 1–40

Heaney PJ, Veblen DR (1991) Observations of the α-β phase transition in quartz: a review of imaging and diffraction studies and some new results. Am Mineral 76: 1018–1032

Heuer AH, Nord GL (1976) Polymorphic phase transitions in minerals. In: Wenk HR (ed) Application of electron microscopy in mineralogy. Springer-Verlag, Berlin Heidelberg New York, pp 271–303

Hobbs LW (1979) Radiation effects in analysis of inorganic specimens by TEM. In: Hren, Goldstein, Joy (eds) Introduction to analytical electron microscopy. Plenum Press, New York, pp 437–480

Krause C, Böhm H (1982) Antiphasendomänen im β-Eukryptit. Z Kristallogr 159: 83–84

Lichtenstein AI, Jones RO, Xu H, Heaney PJ (1998) Anisotropic thermal expansion in the silicate β-eucryptite: a neutron diffraction and density functional study. Phys Rev B 58: 6219–6223

McLaren AC, Phakey PP (1969) Diffraction contrast from Dauphiné twin boundaries in quartz. Phys Status Solidi 31: 723–737

Müller WF, Schulz H (1976) Antiphase domains in β-eucryptite ($LiAlSiO_4$). Naturwissen 63: 294

Nagel W, Böhm H (1982) Ionic conductivity studies on $LiAlSiO_4$-SiO_2 solid solutions of the high quartz type. Solid State Commun 42: 625–631

Nord Jr GL (1992) Imaging transformation-induced microstructures. In: Buseck PR (ed) Minerals and reactions at the atomic scale: transmission electron microscopy. Reviews in Mineralogy, vol 27. Mineralogical Society of America, Washington, DC, pp 453–508

Palmer DC (1994) Stuffed derivatives of the silica polymorphs. In: Heaney PJ, Prewitt CT, Gibbs GV (eds) Silica. Reviews in Mineralogy, vol 29. Mineralogical Society of America, Washington, DC, pp 83–122

Pillars WW, Peacor DR (1973) The crystal structure of beta eucryptite as a function of temperature. Am Mineral 58: 681–690

Press W, Renker B, Schulz H, Böhm H (1980) Neutron scattering study of the one-dimensional ionic conductor β-eucryptite. Phys Rev B 21: 1250–1257

Schönherr E, Schedler E (1977) The growth of β-$LiAlSiO_4$ crystal from high temperature solution in LiF-AlF_3 mixtures. J Crys Growth 42: 289–292

Schulz H (1974) Thermal expansion of beta eucryptite. J Am Ceram Soc 57: 313–317

Schulz H, Tscherry V (1972a) Structural relations between the low- and high-temperature forms of β-eucryptite ($LiAlSiO_4$) and low and high quartz. I. Low-temperature form of β-eucryptite and low quartz. Acta Crystallogr B28: 2168–2173

Schulz H, Tscherry V (1972b) Structural relations between the low- and high-temperature forms of β-eucryptite ($LiAlSiO_4$) and low and high quartz. II. High-temperature form of β-eucryptite and high quartz. Acta Crystallogr B28: 2174–2177

Tscherry V, Laves F (1970) Synthesis and X-ray reflection pattern of β-eucryptite. Naturwissen 57: 194

Tscherry V, Schulz H, Laves F (1972a) Average and super structure of β-eucryptite ($LiAlSiO_4$). Part I, average structure. Z Kristallogr 135: 161–174

Tscherry V, Schulz H, Laves F (1972b) Average and super structure of β-eucryptite ($LiAlSiO_4$). Part II, superstructure. Z Kristallogr 135: 175–198

Van Tendeloo G, Van Landuyt J, Amelinckx S (1976) The α-β phase transition in quartz and $AlPO_4$ as studied by electron microscopy and diffraction. Phys Status Solidi (a) 33: 723–735

Van Tendeloo G, Ghose S, Amelinckx S (1989) A dynamical model for the $P\bar{1}$-$I\bar{1}$ phase transition in anorthite, $CaAl_2Si_2O_8$: I. Evidence from electron microscopy. Phys Chem Minerals 16: 311–319

Williams DB, Carter CB (1996) Transmission electron microscopy. Plenum Press, New York

Winkler HGF (1948) Synthese und Kristallstruktur des Eukryptits, $LiAlSiO_4$. Acta Crystallogr 1: 27–34

Xu H, Heaney PJ (1997) Memory effect of domain structures during displacive phase transitions: a high-temperature TEM study of quartz and anorthite. Am Mineral 82: 99–108

Xu H, Heaney PJ, Yates DM, Von Dreele RB, Bourke MA (1999) Structural mechanisms underlying near-zero thermal expansion in β-eucryptite: a combined synchrotron X-ray and neutron Rietveld analysis. J Mater Res (in press)